Collision Detection and Identification for Robot Manipulators based on Extended State Observer

Tianyu Ren, Yunfei Dong, Dan Wu*, and Ken Chen
State Key Laboratory of Tribology, Department of Mechanical Engineering,
Tsinghua University, Beijing 100084, China

***Abstract*— Physical human-robots cooperation is desirable for future robotic applications while poses the fundamental problem of how to ensure personnel safety. Dynamic impact and quasi-static clamping are two common scenarios that could potentially lead to human injuries and should be detected as sensitive as possible. Combining insights from of the extended state observer (ESO) and robot dynamics, an efficient collision detection method based on only proprioceptive sensors (encoders and torque sensors) is introduced. In addition to detection, the proposed method provides magnitude and direction information of force signals covering a general class of actuator faults. Simulations give a quantitative comparison between the proposed scheme and the widely used method based on general momenta. Experimental results with a 7-DOF collaborative robot further illustrate the effectiveness of the proposed method. The collisions occurring in the form of dynamic impact as well as quasi-static clamping are verified.**

***Keywords*—human-robot interaction; robot manipulator; collision detection; ESO**

1. Introduction

Physical cooperation between human and robot has become a topic of major focus in robotics. A primary concern of a robot designed for cooperation with human or uncertain environment is that it should not pose any threat to human in any cases [1, 2]. The close human-robot interaction (HRI) inevitably lead to physical contact, which is usually divided into two fundamental groups: dynamic loading and quasi-static loading. An overview of the potential injury threats from robot manipulator to human is summarized in [3]. The primary task in safety protection is to detect the collision occurrence and identify its position and magnitude [4].

The existing detection strategies can be separated into two subclasses [5]: model-independent methods and model-based methods. As its name implies, model-independent methods take the advantage of being independent of a specific model. They are generally based on the analysis of signals involved in robot control, such as instantaneous variation of position error or control input signals [6, 7]. These signals are related directly to the structure and parameters of the controllers, so that it is difficult to generalize this class of methods to different control architectures [8]. Benefiting from the progress in machine learning, the detection algorithms based on neural network (NN) [9, 10], support vector machine (SVM) [11] or Fuzzy system [12, 13] reveal an important trend for model-independent methods. These intelligent agents are able to learn to identify accidental collision from labeled data with even less model information. However, none of these algorithms can give a completely accurate prediction of collisions (usually under 95%), and the collection of training data is very problematic in practices.

On the other hand, parameter estimation and observer-based techniques belong to the second class. The detection schemes with parameter estimation rely on the comparison between the predetermined and the identified parameters. Generally，they need appropriate system excitation and thus work only with certain types of impact [14]. Observer-based methods require no special excitation and therefore can handle more scenarios of collision. In addition, most of the observer-based methods are able to work in parallel to the robot controller. These strategies usually comprise two steps: (a) the generation of a diagnostic signals carrying the collision signature, and (b) the comparison between signals and preset thresholds to determine if the fluctuation is due to a collision or just the system noise.

The diagnostic signal is termed as the *residual signal*. In classical model-based methods, residuals are calculated by comparing the current parameter estimates with their nominal values, i.e., the difference between measured and estimated joint torque [14, 15]. As an enhancement of this scheme, the generalized momenta-based (GM) method removes the requirement of acceleration computation and thus significantly reduces the influence of measurement noise [16, 17]. An observer built with an internal state of the generalized momentum $\boldsymbol{p}=\boldsymbol{M}(\boldsymbol{q})\dot{\boldsymbol{q}}$ realizes the collision detection in this scheme. It takes the joint torque, link position, and link velocity as inputs and generates a first-order filtered version of external forces [18]. Based on the idea of torque filter, another method is designed and proves to have the similar benefits of acceleration free as well as controller independence [19].

Due to the intuitive design and reliable performance, the GM method is widely adopted by various robotic applications for safety issues [20-24]. However, in practice, it is found sensitive to modeling errors and disturbances from robot joint actuators.

* Corresponding author.
E-mail address: wud@tsinghua.edu.cn (Prof. D. Wu)
Postal address: Room A829, Lee Shau Kee Science and Technology Building, Tsinghua University, Beijing, 100084, China

The collision detection threshold must be raised to prevent false alarms, which significantly decreases the detection sensitivity. To overcome this problem, a band-pass filter is introduced to separate collision torque from unmodeled dynamic effects and measurement noise [25]. This method is based on the assumption that due to the structure inertia, motion of a robot and its actuators is limited to low frequency. Thus a high pass filter is capable of suppressing those low frequency signals while reserving the abrupt changes resulting from impact [26]. This filtered residual signal can provide a reliable indicator for dynamic impact, while the quasi-static threats like squeezing and clamping are totally overlooked. Furthermore, the band-pass filter may distort the residual signals, which would result in a deformed estimation of the magnitude of contact forces.

This paper is motivated by the requirement of sensitive collision detection and identification in HRI. Starting with the robot dynamic model, the extended state observer (ESO) from the active disturbance rejection control (ADRC) framework is introduced for fast and robust contact force detection. The main contributions of this work are the modified ESO (MESO) algorithm for whole-body collision detection and its application to a practical robot for physical HRI. Residual vectors generated by the MESO contain information of not only the presence, but also the location, magnitude and orientation of a collision. Compared with classical model-based methods, the MESO circumvents the need for acceleration estimation. It is robust to torque disturbances and thus gives residual estimation with more accuracy.

For practical verification, blunt impact experiments with a human volunteer are conducted on a 7-DOF dexterous collaborative robot arm (DCRA) [27] developed by our lab. As well as dynamic collision, we analyze the problem of the quasi-static constrained impact, which poses a serious threat even with lightweight robots. The results prove that the MESO is able to suppress the disturbances from joint actuators and respond rapidly to accidental contacts. We evaluate the collision force during the impact tests and find that with a combination of MESO and the simplest "emergency stop" strategy, the robot is unlikely to cause damage to human in both dynamic and quasi-static collision.

The paper is organized as follows. In Section 2, some preliminaries relative to our study are presented. Section 3 describes the design of the proposed method motivated by the idea of ESO combining the analysis of robot model. To make this paper self-contained, a generalized review of the widely used GM method is included. Section 4 is devoted to the comparison between the MESO and the GM method with respect to the tracking performance in simulation. In Section 5, experiments are carried out to illustrate the effectiveness of the MESO in a collaborative robot concerning quasi-static and dynamic loading. We evaluated the detection sensitivity by using an external force/torque sensor.

2. Preliminaries

2.1. Robot manipulator model

The analytical model for an *n*-degree-of-freedom (DOF) robot manipulator can be written in joint space as the following form:

$$\boldsymbol{M}(\boldsymbol{q})\,\ddot{\boldsymbol{q}} + \boldsymbol{C}(\boldsymbol{q},\dot{\boldsymbol{q}})\,\dot{\boldsymbol{q}} + \boldsymbol{g}(\boldsymbol{q}) = \boldsymbol{\tau} + \boldsymbol{\tau}_{ext} \tag{1}$$

where $\boldsymbol{q}, \dot{\boldsymbol{q}}, \ddot{\boldsymbol{q}} \in \boldsymbol{R}^n$ represent the link angular position, velocity, and acceleration. $\boldsymbol{M}(\boldsymbol{q}) \in \boldsymbol{R}^{n\times n}$ denotes the positive-definite, symmetric inertia matrix. $\boldsymbol{C}(\boldsymbol{q},\dot{\boldsymbol{q}}) \in \boldsymbol{R}^{n\times n}$ and $\boldsymbol{g}(\boldsymbol{q}) \in \boldsymbol{R}^n$ denote the Centripetal-Coriolis and gravitational effects. $\boldsymbol{\tau}_{ext} \in \boldsymbol{R}^n$ is the external torque vector due to physical contact with the environment which could act as an indicator of collision events.

$\boldsymbol{\tau} \in \boldsymbol{R}^n$ is the joint torque generated by robot joint actuators. It can be measured directly from joint torque sensors or inferred by motor currents. It is noteworthy that depending on specific robot controllers, the joint torque may have varying degrees of disturbance from actuators. The actuator in each joint of a robot usually consist of a servo motor and a transmission system with transmission flexibility, motor inertia, and friction [28, 29]

$$\begin{cases} \boldsymbol{B}_a\ddot{\boldsymbol{\theta}} + \boldsymbol{D}_a\dot{\boldsymbol{\theta}} + \boldsymbol{\tau} = \boldsymbol{\tau}_m - \boldsymbol{\tau}_f \\ \boldsymbol{\tau} = \boldsymbol{K}_a(\boldsymbol{\theta} - \boldsymbol{q}) \end{cases} \tag{2}$$

where $\boldsymbol{B}_a$, $\boldsymbol{D}_a$, $\boldsymbol{K}_a \in \boldsymbol{R}^{n\times n}$ are the diagonal, positive definite motor rotor inertia matrices, damping and joint stiffness of the actuator respectively. $\boldsymbol{\tau}_m \in \boldsymbol{R}^n$ represents the electromagnetic torque of motors considered as the system input. $\boldsymbol{\theta} \in \boldsymbol{R}^n$ is the motor positions and it is measured by motor-side encoders. $\boldsymbol{\tau}_f \in \boldsymbol{R}^n$ is the friction torque. Combination of Eq.(1) and Eq.(2) lead to a complex model of flexible joint robot. Instead of working out its mechanism, we consider the actuator dynamics model Eq.(2) as disturbances acting on the dominant rigid robot model Eq. (1) .

The robot model given in Eq. (1) has the following well-known property that is utilized in the subsequent analysis.

Property 1: The matrix $\dot{\boldsymbol{M}}(\boldsymbol{q}) - 2\boldsymbol{C}(\boldsymbol{q},\dot{\boldsymbol{q}})$ is skew-symmetry [30], and so it follows that

$$\dot{\boldsymbol{M}}(\boldsymbol{q}) = \boldsymbol{C}(\boldsymbol{q},\dot{\boldsymbol{q}}) + \boldsymbol{C}^T(\boldsymbol{q},\dot{\boldsymbol{q}})\ . \tag{3}$$

2.2. Strategy of Extended State Observer

As a unique observer design, the extended state observer was originally proposed by Han [31]. The main idea of the observer is to use an augmented state vector for nonlinear disturbance estimation. With consideration of a general model of a second-order MIMO system

$$\ddot{\boldsymbol{y}} = \boldsymbol{f}(t, \boldsymbol{y}, \dot{\boldsymbol{y}}, \boldsymbol{w}) + \boldsymbol{B}\boldsymbol{u}\,, \tag{4}$$

where $\boldsymbol{y} \in \boldsymbol{R}^m$ is the state vector and $\boldsymbol{B}\boldsymbol{u} \in \boldsymbol{R}^m$ is the system input, $\boldsymbol{w} \in \boldsymbol{R}^m$ is an external unknown input, $\boldsymbol{f}$ represents the total disturbance including internal dynamics and external disturbances. Based on the idea of internal state extension, this plant can be augmented as

$$\begin{cases} \dot{\boldsymbol{x}}_1 = \boldsymbol{x}_2 \\ \dot{\boldsymbol{x}}_2 = \boldsymbol{x}_3 + \boldsymbol{B}\boldsymbol{u} \\ \dot{\boldsymbol{x}}_3 = \dot{\boldsymbol{f}}(t, \boldsymbol{y}, \dot{\boldsymbol{y}}, \boldsymbol{w}) \\ \boldsymbol{y} = \boldsymbol{x}_1 \end{cases}, \tag{5}$$

where the total disturbance $\boldsymbol{f}$ is considered as an extended state $\boldsymbol{x}_3$. Here $\boldsymbol{f}$ and its derivative $\dot{\boldsymbol{f}}$ are assumed unknown. Now it is possible to estimate $\boldsymbol{f}$ by using a simple state estimator. The ESO has been shown to be capable of handling different types of nonlinear disturbances without adjusting the structure or parameters [32], and the observer error monotonically decreases with the observer bandwidth [33]. The following property declares the scope of disturbance $\boldsymbol{f}$ that can be estimated by a linear ESO with bounded error.

Property 2: $\lim_{t\to\infty}\|\boldsymbol{E}(t)\|$ is bounded if at least one of the following two conditions is satisfied [32]:

1) $\|\boldsymbol{f}\| \le r_2$, for a constant r_2 at any time.
2) $\|\dot{\boldsymbol{f}}\| \le r_1$, for a constant r_1 at any time.

3. Collision detection and identification method

3.1. Review of the FDI method using generalized momenta

In [16], a method for actuator faults detection and isolation (FDI) has been proposed for robotic systems based on the generalized momenta $\boldsymbol{p} = \boldsymbol{M}(\boldsymbol{q})\,\dot{\boldsymbol{q}}$. It is capable of detecting accidental collision as well as other type of actuator fault, such as free-swinging and saturated actuator fault.

A first-order dynamic equation about $\boldsymbol{p}$ can be written as

$$\dot{\boldsymbol{p}} = \boldsymbol{\tau} + \boldsymbol{\tau}_{ext} + \boldsymbol{C}^T(\boldsymbol{q},\dot{\boldsymbol{q}})\,\dot{\boldsymbol{q}} - \boldsymbol{g}(\boldsymbol{q}). \tag{6}$$

Then by defining the residual vector $\boldsymbol{r}$ as

$$\boldsymbol{r} = \boldsymbol{K}\left[\boldsymbol{p} - \int(\boldsymbol{\tau} + \boldsymbol{C}^T(\boldsymbol{q},\dot{\boldsymbol{q}})\,\dot{\boldsymbol{q}} - \boldsymbol{g}(\boldsymbol{q}) + \boldsymbol{r})dt\right], \tag{7}$$

with $\boldsymbol{K} = \mathrm{diag}\{K_i\} > 0$, a linear system of $\boldsymbol{r}$ driven by the external torque $\boldsymbol{\tau}_{ext}$ is obtained [17].

$$\dot{\boldsymbol{r}} = -\boldsymbol{K}\boldsymbol{r} + \boldsymbol{K}\boldsymbol{\tau}_{ext} \tag{8}$$

Actually, every component of the residual is the filtered version of the external torque. For implementation, a standard observer is always needed to calculate the nonlinear term with measurable outputs only [16]. The GM method is realized as follows.

$$\begin{aligned} &\dot{\hat{\boldsymbol{p}}} = \boldsymbol{\tau} + \boldsymbol{C}^T(\boldsymbol{q},\dot{\boldsymbol{q}})\,\dot{\boldsymbol{q}} - \boldsymbol{g}(\boldsymbol{q}) + \boldsymbol{K}(\boldsymbol{p} - \hat{\boldsymbol{p}}) \\ &\boldsymbol{r} = \boldsymbol{K}(\boldsymbol{p} - \hat{\boldsymbol{p}}) \end{aligned} \tag{9}$$

With this observer, for large values of K_i, the evolution of r_i will reproduce the evolution of contact torque $\tau_{ext,i}$ accurately. However, in most cases, the gain of the observer is limited by modeling error and system noise. The transfer function from joint torque $\boldsymbol{\tau}$ to residual $\boldsymbol{r}$ is a first-order filter that we find in practice cannot provide enough attenuation for the noise in $\boldsymbol{\tau}$. Moreover, the observer is prone to get divergent with inappropriate parameters.

3.2. The extended state observer design

Considering the robot model in Eq. (1), the purpose of collision detection is to calculate the external torque $\boldsymbol{\tau}_{ext}$ rapidly and accurately. In this section, a basic third-order ESO is introduced firstly. Then, by making full use of the system feedback, the observer order is reduced to decrease phase lag. Finally, the resultant second-order ESO is modified in a way that calculation of inverse matrix is no longer needed. Introducing a new variable

$$\boldsymbol{\tau}_a(\boldsymbol{\tau},\boldsymbol{q},\dot{\boldsymbol{q}}) = \boldsymbol{\tau} - \boldsymbol{C}(\boldsymbol{q},\dot{\boldsymbol{q}})\,\dot{\boldsymbol{q}} - \boldsymbol{g}(\boldsymbol{q}), \tag{10}$$

then Eq. (1) can be rewritten as

$$\ddot{\boldsymbol{q}} = \boldsymbol{M}(\boldsymbol{q})^{-1}\boldsymbol{\tau}_a + \boldsymbol{M}(\boldsymbol{q})^{-1}\boldsymbol{\tau}_{ext}. \tag{11}$$

The robot dynamic model is transformed to a second-order integrator with disturbance, wherein $\boldsymbol{M}(\boldsymbol{q})^{-1}\boldsymbol{\tau}_a$ and $\boldsymbol{M}(\boldsymbol{q})^{-1}\boldsymbol{\tau}_{ext}$ are recognized as the system input and total disturbance respectively. Corresponding to the general model in Eq.(4), there is

$$\begin{cases} \boldsymbol{B}\boldsymbol{u} = \boldsymbol{M}(\boldsymbol{q})^{-1}\boldsymbol{\tau}_a \in \boldsymbol{R}^n \\ \boldsymbol{f} = \boldsymbol{M}(\boldsymbol{q})^{-1}\boldsymbol{\tau}_{ext} \in \boldsymbol{R}^n \end{cases} \tag{12}$$

Then a third-order linear ESO is accordingly designed as following

$$\begin{cases} \boldsymbol{e}_o^t = \boldsymbol{z}_1^t - \boldsymbol{q} \\ \dot{\boldsymbol{z}}_1^t = \boldsymbol{z}_2^t - \boldsymbol{\beta}_1\boldsymbol{e}_o^t \\ \dot{\boldsymbol{z}}_2^t = \boldsymbol{z}_3^t - \boldsymbol{\beta}_2\boldsymbol{e}_o^t + \boldsymbol{M}(\boldsymbol{q})^{-1}\boldsymbol{\tau}_a(\boldsymbol{\tau},\boldsymbol{q},\dot{\boldsymbol{q}}) \\ \dot{\boldsymbol{z}}_3^t = -\boldsymbol{\beta}_3\boldsymbol{e}_o^t \end{cases} \tag{13}$$

$$\begin{cases} \boldsymbol{z}_1^t = \hat{\boldsymbol{q}} \\ \boldsymbol{z}_2^t = \hat{\dot{\boldsymbol{q}}} \\ \boldsymbol{z}_3^t = \hat{\boldsymbol{f}} \end{cases} \tag{14}$$

where $\boldsymbol{\beta}_1, \boldsymbol{\beta}_2, \boldsymbol{\beta}_3$ are diagonal matrix containing the gains of the observer, and the hat symbol (^) is used to denote estimated terms. Consequently, $\hat{\boldsymbol{f}} = \boldsymbol{z}_3$ is the estimation of the total disturbance $\boldsymbol{f}$. Then the estimation of external torque is calculated as

$$\hat{\boldsymbol{\tau}}_{ext} = \boldsymbol{M}(\boldsymbol{q})\,\hat{\boldsymbol{f}} \;. \tag{15}$$

Here, in accordance with other FDI methods, the estimation of external torque given by the ESO is also called *residual*. In robot systems, the joint velocity $\dot{\boldsymbol{q}}$ are directly available from the motor drivers. These known system information can be utilized to reduce the order of ESO and further decrease phase lag in observation. Then a reduced-order ESO for collision detection is thus designed as

$$\begin{cases} \boldsymbol{e}_o^r = \boldsymbol{z}_1^r - \dot{\boldsymbol{q}} \\ \dot{\boldsymbol{z}}_1^r = \boldsymbol{z}_2^r - \boldsymbol{\beta}_1\boldsymbol{e}_o^r + \boldsymbol{M}(\boldsymbol{q})^{-1}\boldsymbol{\tau}_a(\boldsymbol{\tau},\boldsymbol{q},\dot{\boldsymbol{q}}) \\ \dot{\boldsymbol{z}}_2^r = -\boldsymbol{\beta}_2\boldsymbol{e}_o^r \end{cases} \tag{16}$$

$$\begin{cases} \boldsymbol{z}_1^r = \hat{\dot{\boldsymbol{q}}} \\ \boldsymbol{z}_2^r = \hat{\boldsymbol{f}} \end{cases} \tag{17}$$

With $\hat{\boldsymbol{f}}$, the residual can be calculated using Eq. (15) in the same way. The reduced-order observer have a higher response speed than the preliminary design, which is critical for safety reaction in HRI. In the above collision observers, it is obliged to calculate the inverse of inertia matrix $\boldsymbol{M}(\boldsymbol{q})$ in each iteration, which is a large computing work especially for multi-degree-of-freedom robots. Therefore, some modification of the algorithm is necessary. In Eq.(16), the inverse inertia matrix is used to acquire the driving signal of the integrator Eq.(11). Therefore, it is natural to think about transforming Eq.(11) into a new differential equation with new internal variables. In order to eliminate $\boldsymbol{M}(\boldsymbol{q})^{-1}$, both sides of Eq. (11) are multiplied by $\boldsymbol{M}(\boldsymbol{q})$ on the left.

$$\boldsymbol{M}(\boldsymbol{q})\,\ddot{\boldsymbol{q}} = \boldsymbol{\tau}_a + \boldsymbol{\tau}_{ext}\,. \tag{18}$$

The term $\boldsymbol{M}(\boldsymbol{q})\,\ddot{\boldsymbol{q}}$ can be obtained by differentiating the general momenta $\boldsymbol{p} = \boldsymbol{M}(\boldsymbol{q})\,\dot{\boldsymbol{q}}$:

$$\dot{\boldsymbol{p}} = \dot{\boldsymbol{M}}(\boldsymbol{q})\,\dot{\boldsymbol{q}} + \boldsymbol{M}(\boldsymbol{q})\,\ddot{\boldsymbol{q}}\;. \tag{19}$$

Combining Eq.(18) and Eq.(19), a first-order differential equation about general momenta can be written as

$$\dot{\boldsymbol{p}} = \boldsymbol{\tau}_p(\boldsymbol{\tau},\boldsymbol{q},\dot{\boldsymbol{q}}) + \boldsymbol{\tau}_{ext}\,, \tag{20}$$

where

$$\boldsymbol{\tau}_p(\boldsymbol{\tau},\boldsymbol{q},\dot{\boldsymbol{q}}) = \dot{\boldsymbol{M}}(\boldsymbol{q})\,\dot{\boldsymbol{q}} + \boldsymbol{\tau}_a \tag{21}$$

is an intermediate variable. According to *Property 1*, $\boldsymbol{\tau}_p$ can be calculated as follows.

$$\boldsymbol{\tau}_p = \boldsymbol{\tau} + \boldsymbol{C}^T(\boldsymbol{q},\dot{\boldsymbol{q}})\,\dot{\boldsymbol{q}} - \boldsymbol{g}(\boldsymbol{q}) \tag{22}$$

Different from the previous two ESO-based methods, this modified ESO has new observer states. Consequently, the correspondence with Eq. (12) is changed to

$$\begin{cases} \boldsymbol{B}\boldsymbol{u} = \boldsymbol{\tau}_p \in \boldsymbol{R}^n \\ \boldsymbol{f} = \boldsymbol{\tau}_{ext} \in \boldsymbol{R}^n \end{cases}. \tag{23}$$

Then, a modified second-order ESO is designed to give estimation of the external torque as

$$\begin{cases} \boldsymbol{e}_o^m = \boldsymbol{z}_o^m - \boldsymbol{p} \\ \dot{\boldsymbol{z}}_1^m = \boldsymbol{z}_2^m - \boldsymbol{\beta}_1\boldsymbol{e}_o^m + \boldsymbol{\tau}_p(\boldsymbol{\tau},\boldsymbol{q},\dot{\boldsymbol{q}}) \\ \dot{\boldsymbol{z}}_2^m = -\boldsymbol{\beta}_2\boldsymbol{e}_o^m \end{cases} \tag{24}$$

$$\begin{cases} \boldsymbol{z}_1^m = \hat{\boldsymbol{p}} \\ \boldsymbol{z}_2^m = \hat{\boldsymbol{\tau}}_{ext} \end{cases} \tag{25}$$

So far, we present three prototypes of external torque observer in a series of optimization: the original ESO, reduced-order ESO (RESO), and finally the modified ESO (MESO). It is interesting to find that the obtained algorithm is similar to that of the GM method [16] with exactly the same observer input (Comparing Eqs. (9) and (24).). Note that the ESO methods employ a higher-order design to give the external torque a proper state for robust estimation, which proves to have a positive effect on the bandwidth improvement with the existence of torque disturbance in robot systems in the following verifications.

Remark: An observer usually works as a low pass filter for the state variable and therefore decreases the noise in feedback loop. However, it also brings undesired phase lag. To ensure a quick response, the delay must be minimized. The presumption of the reduced-order observer is that some of the system state variables are measurable and do not need to be observed. Benefit from the direct measurement of joint velocity in the robot hardware, a faster RESO can evolve from the original. To decrease computation load, further optimization is taken by changing the observer state from the joint velocity $\dot{\boldsymbol{q}}$ to the general momenta $\boldsymbol{p}$. Comparing Eqs. (16) and (24), it is obvious that this modification brings two benefits: first, (a) the calculation of $\boldsymbol{M}(\boldsymbol{q})^{-1}$ is circumvented. Considering that the computational complexity of matrix inversion is a cube of its dimension, this improvement makes the ESO method applicable to robots with even more degrees of freedom; in addition, (b) the lumped disturbance vector given from the ESO is exactly the residual vector for collision detection, eliminating the need for further processing in Eq.(15).

3.3. Dynamics of the collision observer error

In safe robotic applications, not only the occurrence but also the magnitude and location of the physical contact should be identified for safety reaction in higher level. Thus, the observation error, or the difference between residual and actual external torque, is supposed to be bounded in any case.

As the proposed algorithm takes the form of a standard ESO from ADRC scheme, its stability and convergence are naturally guaranteed. Without loss of generality, the error dynamics of MESO is analyzed. Given the observing errors:

$$\begin{cases} \boldsymbol{E}_f = \hat{\boldsymbol{\tau}}_{ext} - \boldsymbol{\tau}_{ext} \\ \boldsymbol{E}_p = \hat{\boldsymbol{p}} - \boldsymbol{p} \\ \boldsymbol{E} = \begin{bmatrix} \boldsymbol{E}_p & \boldsymbol{E}_f \end{bmatrix}^T \end{cases} \tag{26}$$

the error dynamics can be derived from Eqs. (5) and (24):

$$\dot{\boldsymbol{E}} = \boldsymbol{A}\boldsymbol{E} + \boldsymbol{B}\dot{\boldsymbol{f}} \tag{27}$$

where

$$\boldsymbol{A} = \begin{bmatrix} -\boldsymbol{\beta}_1 & \boldsymbol{I} \\ -\boldsymbol{\beta}_2 & 0 \end{bmatrix}, \boldsymbol{B} = \begin{bmatrix} 0 \\ -\boldsymbol{I} \end{bmatrix}. \tag{28}$$

$\boldsymbol{\beta}_1, \boldsymbol{\beta}_2$ are the gains of the ESO parameterized by using a pole-placement method as proposed in [34].

$$\boldsymbol{\beta}_1 = \begin{bmatrix} 2\omega_{o,1} & & \\ & \ddots & \\ & & 2\omega_{o,n} \end{bmatrix},\ \boldsymbol{\beta}_2 = \begin{bmatrix} {\omega_{o,1}}^2 & & \\ & \ddots & \\ & & {\omega_{o,n}}^2 \end{bmatrix} \tag{29}$$

wherein $\omega_{o,i}$ is the observer bandwidth of the *i*-th joint. Further, the observer error of RESO method is obtained by solving Eq. (27).

$$\boldsymbol{E}(t) = e^{\boldsymbol{A}t}\boldsymbol{E}(0) + e^{\boldsymbol{A}t}\int_0^t e^{-\boldsymbol{A}s}\boldsymbol{B}\boldsymbol{f}(s)\mathrm{d}s \tag{30}$$

In most cases, $\boldsymbol{\beta}_1$ and $\boldsymbol{\beta}_2$ are chosen such that $\boldsymbol{A}$ is Hurwitz and has real negative eigenvalues. For the concerned collision types, we assume that the dynamic impact and the quasi-static impact bring step and ramp signals respectively to the external torque. In this case, conditions in *Property 2* are satisfied and thus the boundedness of estimation error is gained. Actually, it is proved in [35] that the estimation error of ESO converges asymptotically when dynamic model is available, and in other cases is bounded with a mostly unknown plant model.

3.4. Collision detection and identification with residual vector

The proposed ESO methods are able to locate robot link with collision and provide directional information on the Cartesian collision force, which is valuable for further safety strategy. Residual $\boldsymbol{r}=\left[r_1 \quad \ldots \quad r_n\right]^T$ from the ESO is the decoupled estimation of $\boldsymbol{\tau}_{ext}=\left[\tau_{ext,1} \quad \ldots \quad \tau_{ext,n}\right]^T$. Contacts in scenarios of HRI will detected when $\|\boldsymbol{r}\|>r_{low}$ or, by working component-wise, when there exists at least one index j for which $\left|r_j\right|>r_{low,j}$, where r_{low} and $r_{low,j}$ are detection thresholds determined by weighing algorithm sensitivity and noise level. When collision occurs on the i-th ($1\le i\le n$) link of the robot kinematic chain, there is

$$\begin{cases} r_1,\ \ldots,\ r_i \ne 0 \\ r_{i+1},\ldots,\ r_n = 0 \end{cases} \tag{31}$$

Within the time interval of contact, the first i components of $\boldsymbol{r}$ are generically different from zero, and will start decaying toward zero as soon as contact is removed. In most cases, the contact forces and location in Cartesian space is more desired for safety investigations and perception fusion with other sensors. The calculation of Cartesian external force from $\boldsymbol{\tau}_{ext}$ is straight-forward by robot kinematics and readers can refer to [36] for details. In this work, we will focus on the technology of external torque estimation and the proposed method is evaluated in joint space.

4. Simulation results

In order to verify the proposed collision detection method, we have considered a 2-DOF planar robot moving in the vertical plane with gravity (Fig. 1).

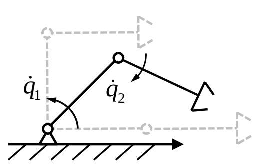

Fig. 1. Considered 2-DOF planar manipulator for simulation. The equilibrium position of the robot movement is shown in dashed lines.

The robot links are assumed to be rods of length 0.4 m with concentrated mass at the rod end of 3.1 kg and 2.1 kg, respectively. The dynamic model takes the form

$$\begin{bmatrix} M_{11} & M_{12} \\ M_{12} & M_{22} \end{bmatrix}\begin{bmatrix} \ddot{q}_1 \\ \ddot{q}_2 \end{bmatrix}+\begin{bmatrix} -C_{12}\dot{q}_2 & -C_{12}(\dot{q}_1+\dot{q}_2) \\ C_{12}\dot{q}_1 & 0 \end{bmatrix}\begin{bmatrix} \dot{q}_1 \\ \dot{q}_2 \end{bmatrix} + \begin{bmatrix} m_1 g_{acc} \\ m_2 g_{acc} \end{bmatrix} = \begin{bmatrix} \tau_1+\tau_{ext,1} \\ \tau_2+\tau_{ext,2} \end{bmatrix}, \tag{32}$$

where

$$\begin{cases} M_{11}=(m_1+m_2)L_1^{\ 2}+m_2L_2^{\ 2}+2m_2L_1L_2\cos(q_2) \\ M_{12}=m_2L_2^{\ 2}+m_2L_1L_2\cos(q_2) \\ M_{22}=m_2L_2^{\ 2} \\ C_{12}=m_2L_1L_2\sin(q_2) \end{cases}, \tag{33}$$

and g_{acc} is the gravitational acceleration. Without loss of generality, it is assumed that the robot motion is controlled by a PID controller with gravitational compensation. According to the technical parameters of the joint 4 and joint 6 of the DCRA, the control signals are input as the motor torques and go through the actuator systems with dynamic parameters of $\boldsymbol{B}_a=\mathrm{diag}(3.701, 0.26)$, $\boldsymbol{D}_a=\mathrm{diag}(0.01, 0.01)$, and $\boldsymbol{K}_a=\mathrm{diag}(32700, 16000)$ [37]. Measurement noise with uniform distribution is artificially added to the motor position feedback with a bound of 2.75×10^{-5}. The manipulator starts at rest in a fully extended configuration and follows square wave inputs. The robot undergoes violent acceleration processes starting at time $\{1,3,5,7\}$ in trajectory tracking (Fig. 2).

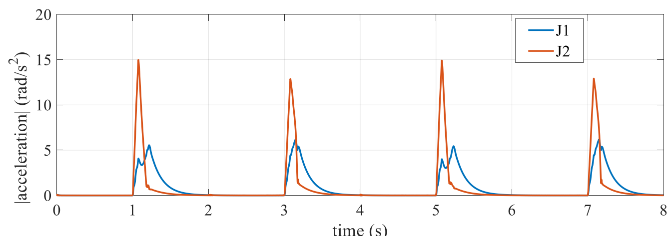

Fig. 2. Acceleration magnitude of the robot joints in simulation.

During the time intervals $[2,4]\cup[7,8]$ s and $[3,7]$ s, intermittent external torques are exerted on the two joints in forms of square wave and triangle wave respectively. So there exists concurrent external torques during $[3,4]$ s. Three residual generation methods, GM, RESO, and MESO, are used to give estimation of the external torques and compare with each other. The simulation environment is built in the Simulink on a workstation with 3.5 GHz quad-core processor and 24 GB memory.

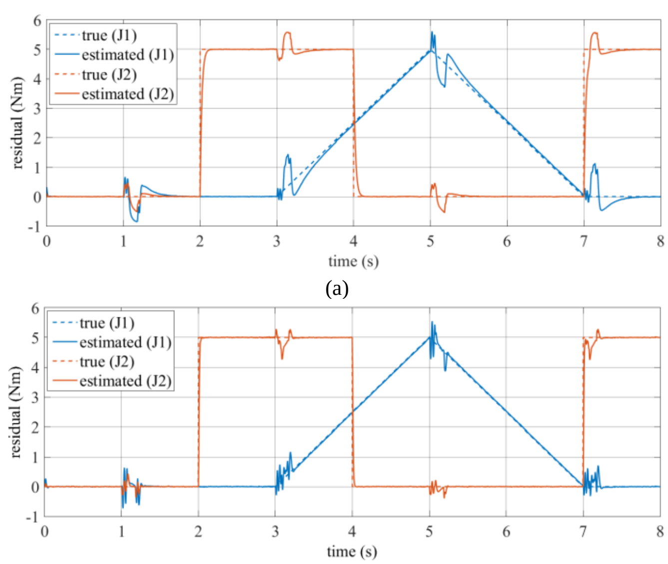

(b)

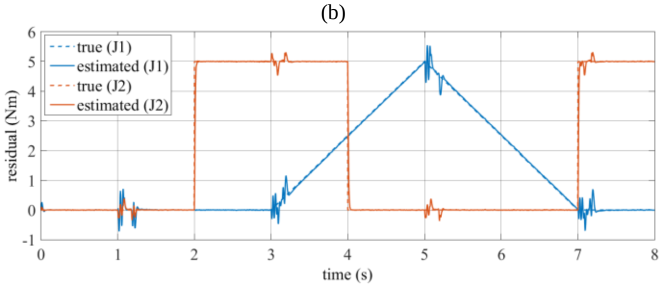

(c)

Fig. 3. Estimation of external torque generated by three detection methods. (a) GM method. The average delay in ramp fault tracking in joint 1 is 24 ms and the rise time in joint 2 is 55 ms. (b) RESO method. The delay in ramp fault tracking is 10 ms and the rise time is 16 ms. (c) MESO method. It has the same bandwidth and performance as the RESO method.

In Fig. 3, the residual evolutions show a practical reconstruction of the external torques and a totally decoupled behavior with the three methods. Figures 2 and 3 show the correspondence between the disturbances in residuals and the joint acceleration. Due to the drastic motor torque as the feedback controller is trying to position the robot, the coupling effect between the rigid body and actuators cause oscillations in residual signals. Notice that in the experiments the gains of the observers are tuned to make a similar noise level in residual signals among three methods. Consequently we have $K_i = 45$ for GM, and $\omega_{o,i} = 200, i = 1, 2$ for RESO and MESO. In general, the ESO methods outperform the GM method in terms of detection performance. While for RESO and MESO, the difference is negligible.

Table.1 contains the specific response performance of the three methods with the computational time in each iteration. Clearly, the MESO has the same performance with the RESO while significantly reduces computational time. On the other hand, the response speed of the MESO is much faster than that of the GM at the expense of a little more computation due to the extended state.

Table 1
Comparison of GM, RESO and MESO method with respect to respond performance and computational time.

Method	Delay in J1	Rising time in J2	Computational time
GM	24 ms	55 ms	11.6 µs
RESO	10 ms	16 ms	26.6 µs
MESO	10 ms	16 ms	15.5 µs

5. Experiments

5.1. Experimental setup

Extensive tests on the proposed method have been performed with the DCRA robot. DCRA has 7 rotary joints with spherical shoulder and wrist axes which are similar to that of a human arm. The maximum load of the robot is 7 kg and its outreach is 1.2 m. It has embedded strain gauge sensors in each joint. Therefore, the state variables (joint torque, position, and velocity) used in the GM and ESO methods can be directly measured. Figure 4 shows the hardware of the DCRA robot prototype. A PC-based controller is used for algorithm implementation. It communicates with drivers and a data acquisition unit through EtherCAT bus with a cycle time of 250 µs.

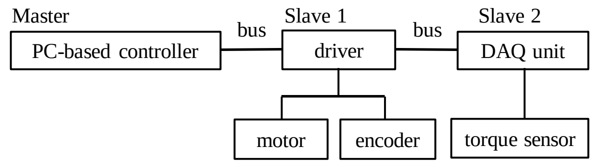

Fig. 4. Hardware structure of the DCRA robot

As stated in Sec. 3, both the GM and MESO methods require the robot dynamic model. In this study, only the rigid robot model is used, while the dynamical behaviors of actuators (i.e., motors and reducers) are considered as disturbances. It is noteworthy that the link positon $\boldsymbol{q}$ and velocity $\dot{\boldsymbol{q}}$ used in the detection algorithms are estimated by the motor-side measurements $\boldsymbol{\theta}, \dot{\boldsymbol{\theta}}$ as they are available for most robot manipulators. Coincident with the simulation, the observer bandwidth of MESO is chosen as $\omega_{o,i} = 200$ for all seven joints.

5.2. Comparison between the MESO and the GM method

First, we verify the capability of the proposed observer to distinguish collision from internal inertia force. The MESO is implemented on DCRA, and the detection results are compared to that of the GM method. During the tests, the robot revolves its first joint back and forth with the large inertia of its body. The trajectory is designed with a maximum acceleration of 280 °/s^2 and a maximum velocity of 60 °/s. The robot collide with a cushion held by a human user for two times respectively within the cruise phase and acceleration phase of movement (see Fig. 5). Note that in this experiment, no reaction will be taken when collision occurs, and the robot will continue its movement after bouncing off the cushion.

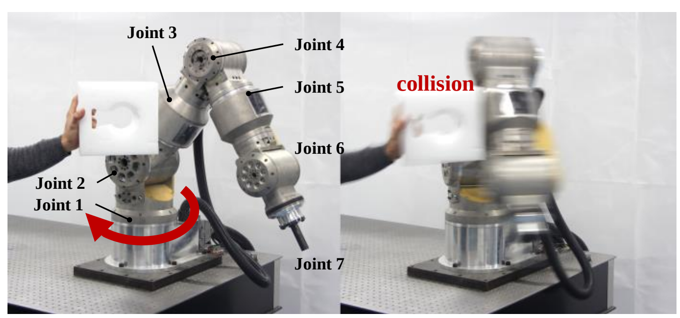

Fig. 5. Dynamic impact test on the DCRA robot prototype for performance comparison of the ESO and the GM method. No reaction will be taken by the robot if collision is detected.

The parameters of the GM method are chosen to ensure that the noise level is comparable to MESO. Figure 6 shows the residuals generated by the MESO and GM method with the measured torque in the first joint. In the cruise phase, the inertia force is trivial. It is reasonable to consider that any spikes in the joint torque result from physical impacts. While in the acceleration phase, the joint torque becomes a lumped signal superposed by inertia force and contact force. It is not easy to recognize intuitively a simple impact from these lumped torque signals. The two observers give clear collision identifications in both kind of phase and the residuals are filtered from the torque signals. On the other hand, it is clear that the residual from the MESO raises to a higher value during the two impacts compared with that of the GM method. In the cruise phase of 0.5 to 1.5 s, the joint torque is considered as the reference signal to evaluate the estimation error of the two methods (see Fig. 7). The estimation RMS values during this episode are 6.89 and 5.36 respectively for GM and MESO. Observations from Figure 6 and 7 reveal a faster response as well as a more accurate estimation of external torque with the MESO method.

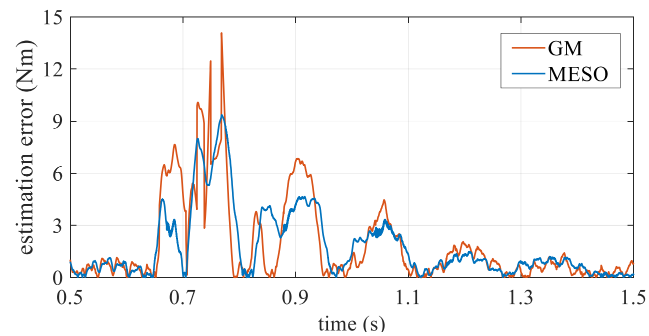

Fig. 7. Estimation error of the GM and MESO method (Impact 1 in Fig. 6). The measured joint torque is used as the reference signal. The estimation RMS values during this episode are 6.89 and 5.36 respectively for GM and MESO.

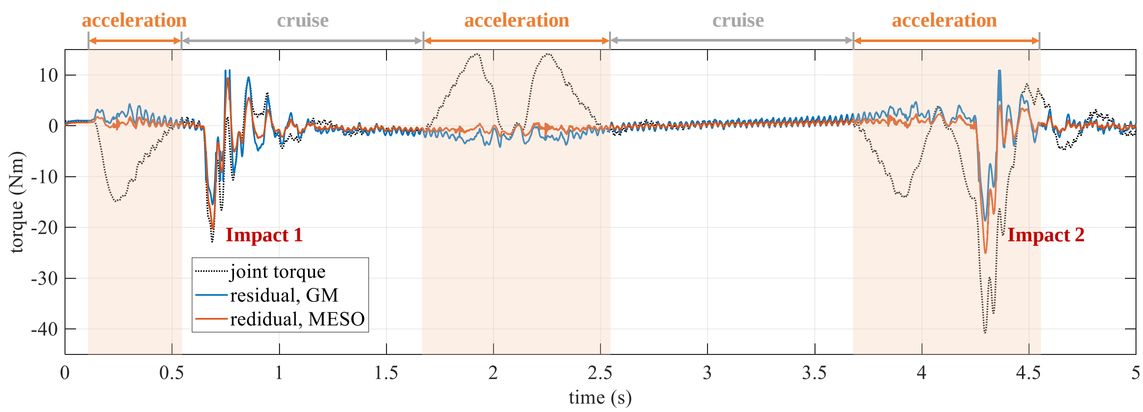

Fig. 6. Comparison of the measured torque of the joint 1 and the residual signals generated by GM method and MESO method. Impacts occurs in the cruise phase as well as the acceleration phase.

6. Applications in human-robot interaction scenarios

6.1. Dynamic impact detection

The dynamic impact is the first injury mechanism investigated in previous robotics literatures, and is extensively used to verify the collision detection and reaction strategy of robot systems [18]. Although it is concluded in [3] that no physical collision detection and reaction strategy is fast enough to reduce the impact force of fast and rigid unconstraint impacts, absolute rigid part does not exist in a human body (even with the human head). Therefore, any deformation of the human body can prolong contact time such that active safety mechanisms have the chance to avoid further squeezing. In order to show the effectiveness of the proposed collision detection method, dynamic impact tests are conducted on DCRA with a non-clamped human arm. As soon as the collision is detected, the robot stops its movement in emergency.

The test trajectory is designed to cover two representative robot movements that are very likely to cause collisions: rotating around the waist (joint 1), and stretching out from a bent configuration. Thus, a path is assigned to the joint 1, joint 2 and joint 4 of the robot with the maximum angular velocities of 75 °/s, 40 °/s, and 80 °/s, respectively, as shown in Fig. 8.

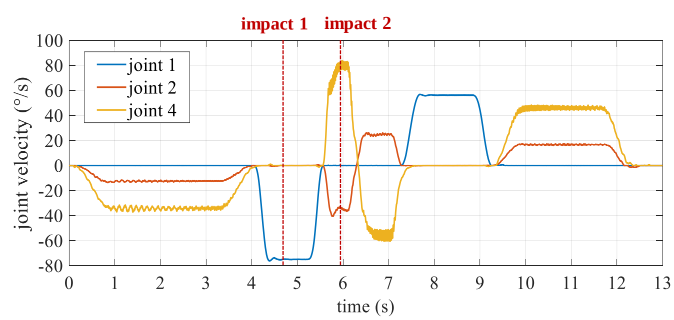

Fig. 8. Velocity profile designed for the two dynamic impact tests. Motion was assigned to the joint 1, joint 2 and joint 4 of the 7-DOF robot. The dashed lines indicate two impact point of this trajectory in two collision tests.

Before the introduction of impacts, the robot runs the designed trajectory in free space. The residuals generated by the MESO are observed to determine the threshold for collision detection. Figure 9 shows the residuals with the measured torque signals of the three joints during this unconstraint movement. Though there exists some noise resulting from the actuator systems, the MESO manages to keep the residuals near zero in spite of the dynamic force of the robot body. Then the collision threshold is set at 10 % of the maximum output torques available at each joint: 15 Nm, 15 Nm and 8 Nm for joint 1, joint 2 and joint 4 respectively.

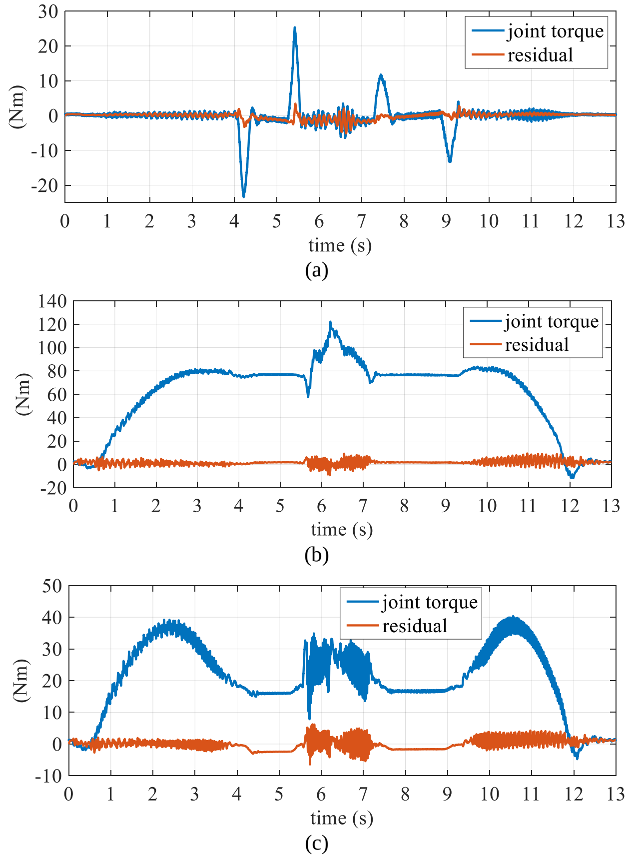

Fig. 9. Residual and joint torque signal of each joint in the trajectory designed for dynamic impact test. There is no collision happening.(a) the joint 1, (b) the joint 2, and (c) the joint 4.

The collision points on the robot body are selected at the end-effecter, so that a 6-DOF Force/Torque (F/T) sensor (ATI Mini40 SI-80-4) mounted at the end can be used to measure the contact force. This sensor is not used for detection, but only for validation purposes. Figure 9 shows the impact positions of the two experiments. During the experiments, the human keeps still and relaxed with his forearm placed at the impact positions ahead of time.

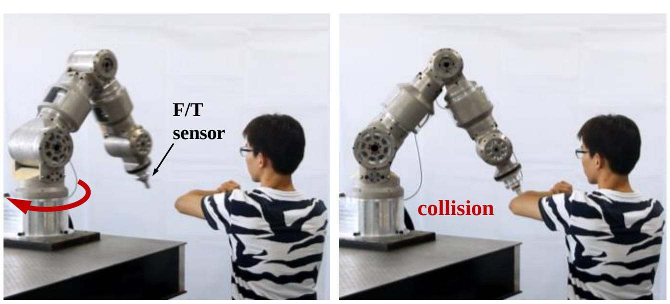

(a)

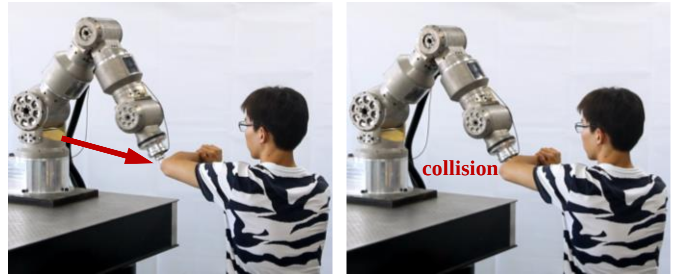

(b)

Fig. 10. Collision detection experiment of dynamic impact. The robot collides with human arm in two test scenarios within the designed trajectory. (a) The robot rotates around joint 1 and hits human arm at a TCP speed of 0.9 m/s. (b) The robot impacts human arm at a TCP speed of 0.5 m/s with its arm outstretch forward.

The robot repeats the preset trajectory two times and collides with the human arm at two different points respectively with the TCP (Tool Center Point) velocity of 0.9 m/s and 0.5 m/s respectively (see Fig. 8). In the first impact test, the contact force, joint torques (Fig. 11a), and the resulting residuals (Fig. 11b) are documented. In this scenario, as the moment of impulse with respect to the joints 2 and 4 is zero, only joint 1 responds to the collision. The residual of joint 1 rises to its threshold in 30 ms and triggers the brake action of DCRA. Taking advantage of the decoupling characteristic of the ESO-based methods, we can estimate the impact vector from the available residual signals with current robot configuration. As soon as contact is lost, the contact force and the residual start to decay toward zero. As it is shown in Fig. 11a, the propagation of the impulse over the robot inertia and the intrinsic joint elasticity leads to a considerable delay in the joint torque in relation to the contact force.

Figure 12 shows the contact force and the residuals in the second impact test. Joints 2 and joint 4 are able to perceive the collision in this configuration. Note that the two residual signals do not rise simultaneously with a single impact excitation because of the impulse propagation. It took about 20 ms for the residual of the joint 4 to reach its threshold, while the collision is detected by the joint 2 about 10 ms later.

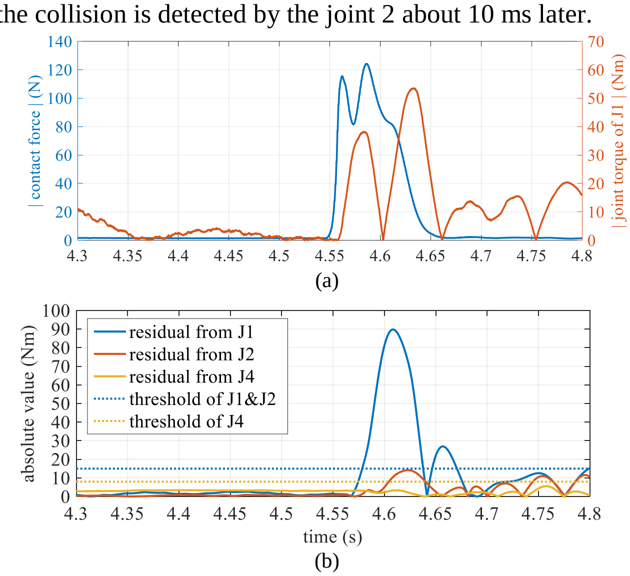

Fig. 11. The first test scenario of dynamic impact. (a) Illustration of the delay between the peak of contact force and that of joint torque. (b) Residual and detection threshold of each joint. Collision is detected by the joint 1.

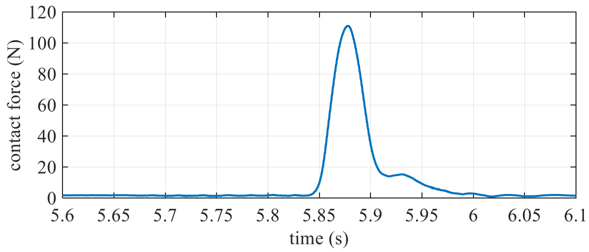

(a)

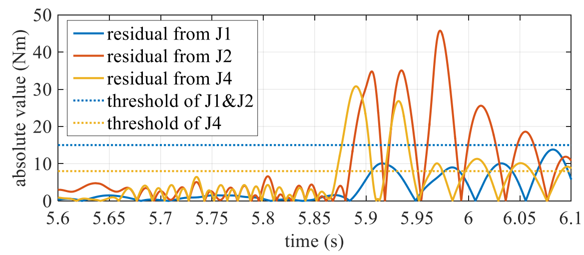

(b)

Fig. 12. The second test scenario of dynamic impact. (a) Magnitude of contact force. (b) Residual and detection threshold of each joint. Collision is detected by the joint 4 and the joint 2 in succession.

Though the MESO method may take some time to respond to the peak of contact force, with the combination of this method and a simple "emergency stop" strategy, the force peaks last no more than 100 ms and stay under 120 N in the two impact tests. According to the collaborative operation requirements for industrial robots from ISO10218 [38]: the maximum static force at most 150 N, this robot system seems not to cause severe damage (as fracture) to human body. In addition to quantitative measures by the F/T sensor, however, the experience of the human operator indicates a high safety awareness.

6.2. Quasi-static impact detection

Getting hands or other parts of body locally clamped by robot manipulators can be very dangerous when the contact force is not limited properly. Clamping or squeezing will lead to slow changing residuals which is generally overlooked by filter-based detection methods [25]. In this experiment, the detectability of the MESO for quasi-static impact is verified on DCRA. The minimal detected force in the elbow joint is experimentally evaluated for the potential squeezing injury from the angle between the upper arm and forearm of the robot.

Joint 4 of DCRA moves according to a trapezoidal velocity profile with cruise speed of 10 °/s. The forearm moves downward in vertical plane until a collision occurs between the robot limb and an elastomer. A 6-DOF F/T sensor is placed under the elastomer to measure the contact force (Fig. 13). The detection threshold is kept unchanged from the previous experiment that is 15 Nm for joint 4.

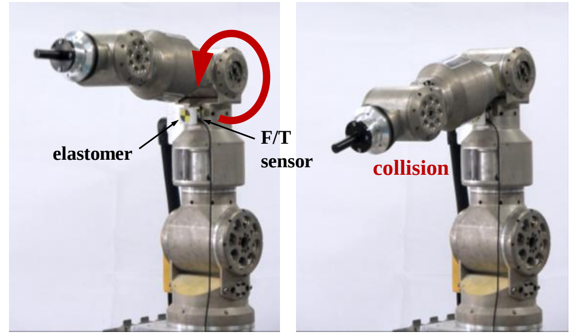

Fig. 13. Collision detection experiment of quasi-static impact. The elbow joint (joint 4) of robot clamps an F/T sensor at a constant speed of 10 °/s. The F/T sensor is covered by an elastomer to simulation the inherent flexibility of human body.

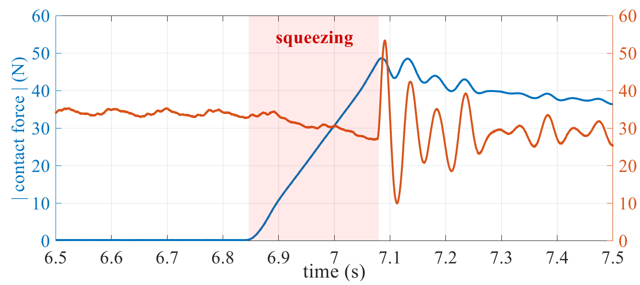

(a)

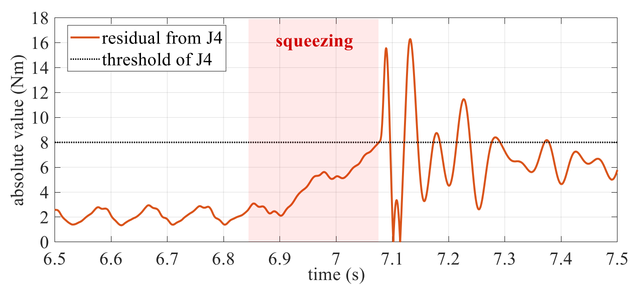

(b)

Fig. 14. Experimental results of the proposed collision detection method for quasi-static impact. (a) Contact force changed slowly within the squeezing phase, and so does the joint torque. (b) Residual begins to increase as soon as the clamping occurs and finally reaches the collision threshold.

Figure 14 illustrates the contact force and joint torque (Fig. 14a) with the residual generated by the MESO (Fig. 14b). Before the collision, the joint torque is a reflection of gravitational force and further depends on the robot configurations. Then the gradual increase in squeezing force leads to a slowly rising residual signal. Finally, the "emergency stop" is triggered when the residual rise to the threshold. Though the collision point is selected close to the elbow joint so that the arm of force is quite short, a clamp force as small as 48 N can be detected, which is unlikely to hurt any parts of a human body. Therefore, it is shown that a compression in quasi-static state can be efficiently detected by the propose method.

In the two safety applications above, the MESO method mainly shows its capacity for collision detection. However, the residual signals contains information of not only the appearance of the impact but also its position, direction and form: (a) with the help of the decoupled estimation of external torques, we are able to derive intuitively the location and direction of a collision. In the first test of dynamic impact experiment, only the residual of joint 1 raised significantly for the collision. Therefore, it is directly perceived that the direction of collision force is parallel to the axes of the joint 2 and the joint 4. In the second test, from the nonzero output of joint 2 and joint 4 and the quasi-zero output of joint 1, the external force vector can be speculated lying in the configuration plane of the robot. According to robot kinematics, the exact directions can be calculated as stated in Sec. 3.4, which is beyond the scoped of this research. (b) Benefit from the extended state for external torques in the observer, the MESO can provide accurate estimation of contact forces with limited error, so that it is able to recognize different types of collision from the profile of residual signals (e.g. dynamic impact from Figs. 10 and 11; quasi-static squeezing from Fig. 13). Therefore practical collision identification can be realized with the proposed method, while actually it has been achieved in joint space.

7. Conclusion

In this paper, we present a new collision detection method for multi-joint robots. Starting from the original ESO used for closed-loop control, a collision observer is designed iteratively through order reduction and reselection of observer variables for computational efficiency.

The use of MESO provides a natural and efficient method for detecting and identifying collision in robot systems, without the need of estimating joint acceleration or inverting the inertia matrix. Compared to the well-known GM method, the MESO is able to provide better estimation of the collision force with similar noise level in practical systems. Though the extra state for external torque leads to slightly increased computation and potential observation delay, it is essential to suppress the significant disturbances from actuators and therefore ensure a high bandwidth of the observer. This method is general enough to handle the common dynamic impact as well as the quasi-static impact. In fact, the residual vector involve richer information about both the robot dynamics and the external loads. As a result, future work is to extract the valuable knowledge from the residual and design collision reaction strategy based on it. On the other hand, the MESO should be enhanced with adaptability to the uncertainties in the robot model.

8. Acknowledgement

The authors gratefully acknowledge financial support from the National Nature Science Foundation of China [Grant No. 51575306] and the Siemens Ltd., China.

References

[1] J. Heinzmann and A. Zelinsky, "Quantitative Safety Guarantees for Physical Human-Robot Interaction," *International Journal of Robotics Research*, vol. 22, no. 7-8, pp. 479-504, 2003.

[2] K. Ikuta, H. Ishii, and M. Nokata, "Safety Evaluation Method of Design and Control for Human-Care Robots," *International Journal of Robotics Research*, vol. 22, no. 5, pp. 281-298, 2003.

[3] S. Haddadin and G. Hirzinger, *Requirements for Safe Robots: Measurements, Analysis and New Insights*. Sage Publications, Inc., 2009, pp. 1507-1527.

[4] S. Haddadin, A. D. Luca, and A. Albu-Schäffer, "Robot Collisions: A Survey on Detection, Isolation, and Identification," *IEEE Transactions on Robotics*, vol. PP, no. 99, pp. 1-21, 2017.

[5] M. Hilbe *et al.*, "Observer-based supervision and fault detection in robots using nonlinear and fuzzy logic residual evaluation," *IEEE Transactions on Control Systems Technology*, vol. 4, no. 3, pp. 274-282, 1996.

[6] H. W. Je, J. Y. Baek, and C. L. Min, "Current based compliance control method for minimizing an impact force at collision of service robot arm," *International Journal of Precision Engineering & Manufacturing*, vol. 12, no. 2, pp. 251-258, 2011.

[7] B. J. Jung, J. C. Koo, H. R. Choi, and H. Moon, "Human-robot collision detection under modeling uncertainty using frequency boundary of manipulator dynamics," *Journal of Mechanical Science & Technology*, vol. 28, no. 11, pp. 4389-4395, 2014.

[8] M. Makarov, A. Caldas, M. Grossard, P. Rodriguez-Ayerbe, and D. Dumur, "Adaptive Filtering for Robust Proprioceptive Robot Impact Detection Under Model Uncertainties," *IEEE/ASME Transactions on Mechatronics*, vol. 19, no. 6, pp. 1917-1928, 2014.

[9] A. N. Sharkawy, P. Koustoumpardis, and N. A. Aspragathos, *Manipulator Collision Detection and Collided Link Identification based on Neural Networks*. 2018.

[10] A. C. Silva, J. Silva, and C. P. D. Santos, "A Modified LGMD Based Neural Network for Automatic Collision Detection," vol. 283, pp. 217-233, 2014.

[11] K. Narukawa, T. Yoshiike, K. Tanaka, and M. Kuroda, "Real-time collision detection based on one class SVM for safe movement of humanoid robot," in *Ieee-Ras International Conference on Humanoid Robotics*, 2017, pp. 791-796.

[12] F. Dimeas, L. D. Avendañovalencia, and N. Aspragathos, "Human - robot collision detection and identification based on fuzzy and time series modelling," *Robotica*, vol. 33, no. 9, pp. 1886-1898, 2015.

[13] J. Xia, G. Wu, C. Li, and H. Liu, "Real-time collision detection for manipulators based on fuzzy synthetic evaluation," in *IEEE International Conference on Mechatronics and Automation*, 2016, pp. 777-782.

[14] B. Freyermuth, "An approach to model based fault diagnosis of industrial robots," in *IEEE International Conference on Robotics and Automation, 1991. Proceedings*, 1991, pp. 1350-1356 vol.2.

[15] F. Caccavale and I. D. Walker, "Observer-based fault detection for robot manipulators," in *IEEE International Conference on Robotics and Automation, 1997. Proceedings*, 1997, pp. 2881-2887 vol.4.

[16] A. De Luca and R. Mattone, "Actuator failure detection and isolation using generalized momenta," in *IEEE International Conference on Robotics and Automation, 2003. Proceedings. ICRA*, 2003, pp. 634-639 vol.1.

[17] A. D. Luca, A. Albu-Schaffer, S. Haddadin, and G. Hirzinger, "Collision Detection and Safe Reaction with the DLR-III Lightweight Manipulator Arm," in *Ieee/rsj International Conference on Intelligent Robots and Systems*, 2007, pp. 1623-1630.

[18] S. Haddadin, A. Albu-Schaffer, A. D. Luca, and G. Hirzinger, "Collision detection and reaction: A contribution to safe physical Human-Robot Interaction," in *Ieee/rsj International Conference on Intelligent Robots and Systems*, 2008, pp. 3356-3363.

[19] W. E. Dixon, I. D. Walker, D. M. Dawson, and J. P. Hartranft, "Fault detection for robot manipulators with parametric uncertainty: a prediction-error-based approach," *Robotics & Automation IEEE Transactions on*, vol. 16, no. 6, pp. 689-699, 2000.

[20] C. Cho, J. Kim, Y. Kim, J. Song, and J. Kyung, "Collision Detection Algorithm to Distinguish Between Intended Contact and Unexpected Collision," *Advanced Robotics*, vol. 26, no. 16, pp. 1825-1840, 2012.

[21] S. D. Lee, Y. L. Kim, and J. B. Song, "Novel collision detection index based on joint torque sensors for a redundant manipulator," in *Ieee/rsj International Conference on Intelligent Robots and Systems*, 2014, pp. 4636-4641.

[22] A. D. Luca and R. Mattone, "Sensorless Robot Collision Detection and Hybrid Force/Motion Control," in *IEEE International Conference on Robotics and Automation*, 2006, pp. 999-1004.

[23] A. De Luca, F. Flacco, A. Bicchi, and R. Schiavi, "Nonlinear decoupled motion-stiffness control and collision detection/reaction for the VSA," in *Ieee/rsj International Conference on Intelligent Robots and Systems*, 2009, pp. 5487-5494.

[24] Y. Tian, Z. Chen, T. Jia, A. Wang, and L. Li, "Sensorless collision detection and contact force estimation for collaborative robots based on torque observer," in *IEEE International Conference on Robotics and Biomimetics*, 2017, pp. 946-951.

[25] C. N. Ho and J. B. Song, "Collision detection algorithm robust to model uncertainty," *International Journal of Control Automation & Systems,* vol. 11, no. 4, pp. 776-781, 2013.

[26] S. D. Lee and J. B. Song, "Collision detection of humanoid robot arm under model uncertainties for handling of unknown object," in *Ieee-Ras International Conference on Humanoid Robots*, 2015, pp. 718-721.

[27] T. Ren, Y. Dong, D. Wu, G. Wang, and K. Chen, "Joint Torque Control of a Collaborative Robot Based on Active Disturbance Rejection With the Consideration of Actuator Delay," in *ASME 2017 International Mechanical Engineering Congress and Exposition*, 2017, p. V04AT05A010.

[28] M. W. Spong, "Modeling and control of elastic joint robots," *Journal of dynamic systems, measurement, and control,* vol. 109, no. 4, pp. 310-319, 1987.

[29] M. W. Spong, M. Vidyasagar, H. Pota, and T. Alberts, "Robot dynamics and control," *IEEE Transactions on Automatic Control,* vol. 39, no. 8, pp. 1774-1775, 1994.

[30] F. L. Lewis, C. T. Abdallah, and D. M. Dawson, "Control of robot manipulators," pp. 251-272, 1993.

[31] J. Han, "From PID to active disturbance rejection control," *IEEE transactions on Industrial Electronics,* vol. 56, no. 3, pp. 900-906, 2009.

[32] X. Yang and Y. Huang, "Capabilities of extended state observer for estimating uncertainties," in *American Control Conference, 2009. ACC'09.*, 2009, pp. 3700-3705: IEEE.

[33] W. Zhou, S. Shao, and Z. Gao, *A Stability Study of the Active Disturbance Rejection Control Problem by a Singular Perturbation Approach*. 2009, pp. 491-508.

[34] Z. Gao, "Scaling and bandwidth-parameterization based controller tuning," in *Proceedings of the American control conference*, 2006, vol. 6, pp. 4989-4996.

[35] Q. Zheng, L. Q. Gao, and Z. Gao, "On Estimation of Plant Dynamics and Disturbance from Input-Output Data in Real Time," in *IEEE International Conference on Control Applications*, 2007, pp. 1167-1172.

[36] B. S. Eberman and K. Salisbury, "Whole-Arm Manipulation: Kinematics and Control," *Massachusetts Institute of Technology,* 1989.

[37] M. Spong, K. Khorasani, and P. Kokotovic, "An integral manifold approach to the feedback control of flexible joint robots," *IEEE Journal on Robotics & Automation,* vol. 3, no. 4, pp. 291-300, 1987.

[38] B. S. Institution, "Robots and robotic devices : safety requirements for industrial robots," 2011.